Effect of disorder on the optical properties of colloidal crystals

Rajesh Rengarajan and Daniel Mittleman*
Department of Electrical and Computer Engineering, Rice University, MS-366, P.O. Box 1892, Houston, Texas 77251, USA

Christopher Rich and Vicki Colvin
Department of Chemistry, Rice University, MS-60, P.O. Box 1892, Houston, Texas 77251, USA
(Received 21 April 2004; published 25 January 2005)

Colloidal crystals offer a promising route for the formation of three-dimensional photonic crystals. The primary constraint in working with these materials is the disorder present in these self-assembled materials. Sphere vacancies, line dislocations, and random position errors all lead to a degradation in the optical properties. It is important to characterize these effects so as to guide further developments in colloidal crystal optics. Here, we report a systematic and quantitative study of disorder in colloidal crystals with visible diffractive properties. Using optical spectroscopy and digital imaging we have correlated several measures of structural disorder with variations in the transmissive and reflective optical properties. We observe a critical size distribution above which rapid deterioration of the lowest stop band is observed. Below this critical size distribution, we observe excellent optical quality, nearly independent of the size distribution. Single sphere vacancies also increase in crystals formed from more polydisperse spheres. The primary effect of this type of defect is to increase the broadband diffuse scattering.

DOI: 10.1103/PhysRevE.71.016615 PACS number(s): 42.70.Qs, 61.72.Dd, 81.16.Dn

I. INTRODUCTION

For many years photonic band gap materials have provided scientists with diffractive systems rich in complex physics and chemistry [1–3]. These materials exhibit dielectric periodicity in one, two or three dimensions. As a result of this periodicity, electromagnetic waves of certain frequencies have no propagating modes within the material. This results in a gap in the photonic band structure. Three-dimensional photonic crystals are especially valuable for applications that exploit the complete confinement of light, such as the inhibition of spontaneous emission [1]. Lithography provides an ideal tool for forming high quality one and two-dimensional crystals for applications such as wave-guiding, wavelength multiplexing, cavity quantum electrodynamics, filtering and optical switching [4–14]. However, such structures, which rely on waveguide effects for confinement in the remaining dimensions, can suffer from excessive leakage losses [15]. In addition, lithographic or "top-down" approaches are relatively expensive and time-consuming processes; the generation of arbitrary three-dimensional structures is especially problematic for a top-down fabrication strategy [16].

In contrast, chemical assembly of ordered dielectrics provides a simpler and less costly approach to generating large-scale photonic crystals [17–26]. These techniques make use of the spontaneous assembly of submicron particles into specific well-ordered lattice structures. These colloidal lattices have been used as templates to create periodic structures using a wide variety of materials, including semiconductors [19,27–32], insulators [33,34], and even metals [35–39]. Recently techniques in substrate patterning and soft lithography have been combined with colloidal crystal fabrication. This has permitted the control of lithographic approaches to be combined with the ease of preparation of the self-assembly methodology [40–45].

In this paper we fabricate colloidal crystals using controlled drying, a widely employed method for crystal formation also known as convective self-assembly [23,26,44,46]. This technique, which has largely supplanted gravity sedimentation as the preferred method for colloidal crystal formation, produces single-crystal planar films of colloidal crystals over large areas, with precise control over the film thickness. Colloids in a liquid suspension are drawn up into a solvent meniscus where they order and pack into a face-centered cubic (fcc) array under the influence of surface tension forces [23]. A vertical glass slide acts as a substrate on which this photonic crystal lattice is deposited. As the solvent evaporates and the meniscus drops with respect to the glass slide, the colloidal crystal is continuously deposited on the substrate.

In the controlled drying method, there are several factors that are critical to the formation of a uniform, well ordered crystal. It has been shown that the evaporation rate, the particle flux, the wetting of the substrate and the meniscus properties are important control parameters [47]. Though the dynamics of the process are not completely understood, it is clear that self-assembly has the potential for inefficient packing leading to imperfect crystal formation.

The promise in using controlled drying methods to fabricate photonic crystals lies in the economy and ease associated with the manufacturing process, as well as the diverse array of material systems that can be formed from colloidal crystal templates. An important challenge for this method is the reduction in the number of crystal defects generated during thin film growth. Typical defects may include line defects, point defects, drying cracks, stacking faults and random variations in the sphere positions. These defects perturb the structural periodicity of the photonic crystal, and can

*Corresponding author. Email address: daniel@rice.edu

therefore alter their optical performance. Several theoretical treatments suggest that though the full photonic band gap (between the 8th and 9th bands) is extremely sensitive to any disruption in the periodicity of the photonic crystal lattice, the lower energy pseudogap (between bands 2 and 3) is only moderately sensitive to crystal defects [48,49]. A quantitative experimental evaluation of the sensitivity of the optical properties to these defects, however, is still lacking. Such information is vital to developing colloidal crystals as optical devices, as well as for determining the level of perfection required for particular applications.

There have been several studies, both theoretical [48–51] and experimental [52–57], which have investigated specific defects in gravity-sedimented, shear aligned [25] and dispersed [58–60] colloidal crystals, and their connection to the optical properties. As expected, the presence of defects correlates with a diminished reflectivity inside the stop band. However, in those cases it was not possible to systematically evaluate the role of defects in the optical properties. In particular, crystals grown from gravity sedimentation form with many grain boundaries, and are in effect polycrystalline. By contrast, the thin films described here are single crystals with few grain boundaries [23].

Clearly, the origin of many of the defects in colloidal crystals is the nonuniformity in the size of the spherical colloids. This fact suggests an interesting method for experimentally controlling the quality of the colloidal crystal films. By using colloids with a range of well-characterized size distributions, we can fabricate films with a range of crystalline order. It has been theoretically demonstrated that the band gap, as determined from the density of states, is more sensitive to size randomness in the colloidal particles than to site randomness [49]. This suggests that the monodispersity of the colloids is the critical factor in determining the quality of a photonic crystal. Also, the size dispersion of the colloidal particles has a direct effect on the structural quality of the crystal; a crystal made from colloids having a large size distribution, for example, will not pack into a well-ordered close-packed lattice. Just as it is hard to stack billiard balls of uneven size, it is difficult to obtain a perfect close-packed lattice with spheres having a large size distribution. Even one large sphere in a uniform lattice can cause local changes in the positions of neighboring colloidal sites [46].

The aim of this work is to evaluate the role of disorder in determining the quality of a photonic crystal. We describe quantitative methods to characterize disorder in colloidal crystals and correlate the structural quality with the optical quality. This data permits us to determine how much disorder can be tolerated in a sample before significant departures from the properties of the ideal crystal are observed. The goals are to determine what level of structural order can be achieved with near perfect colloids and how this structural order degrades when imperfect colloids are used for film formation. Optical methods provide the ideal tools for monitoring the quality of the crystals and thus enable a correlation between colloidal sphere monodispersity and photonic behavior to be established.

II. EXPERIMENT

In this work we studied assembled crystals of silica colloids. Figure 1 shows the photonic band structure [61] for a face-centered cubic close-packed crystal of silica colloids with refractive index $n=1.38$ [62]. Colloids arranged in a face-centered cubic (fcc) lattice possess a pseudogap at a scaled frequency $\omega a/2\pi c=0.48$, where a is the lattice parameter of the primitive cell, equal to the sphere diameter. This is attributed primarily to scattering from the [111] planes, oriented parallel to the substrate. Although it is well known that silica colloidal crystals have no full photonic band gap, they are nonetheless the starting point from which high index contrast macroporous photonic structures (which can have a full gap) are fabricated [63–65]. Samples with higher index contrast are formed using templating techniques, which involve intercalating materials into the interstitial regions of the close-packed silica sphere arrays, and then removing the spheres by chemical etching [19,21,34,66–71]. This permits the fabrication of inverse structures which retain the precise crystalline geometry of the starting film. Since templating preserves not only the crystal structure but also all of the lattice defects of the template, the structural properties of the template dictate the properties present in the final architectures. For this reason, we have exclusively studied films consisting of close-packed arrays of silica colloids, which consist of silica spheres surrounded by air.

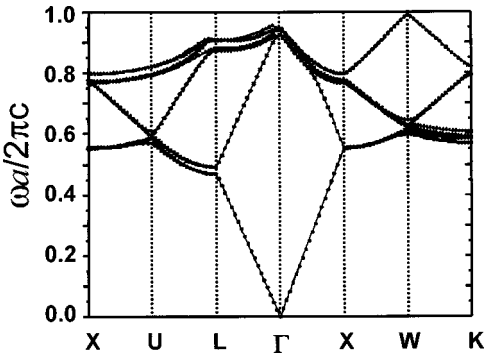

FIG. 1. Photonic band structure [61] for an fcc crystal of close-packed silica colloids, with refractive index $n=1.38$. The lowest 10 energy bands are shown.

Using Stober's method, numerous suspensions of silica colloids were prepared [72]. Colloidal crystals from these suspensions were prepared using the controlled drying technique discussed above, described in detail elsewhere [23]. The crystals were grown in a plexiglass chamber containing a dehydrating agent in order to keep the humidity levels low (8–12 %). We have found that colloidal crystals grown from ethanol suspensions are less uniform if there is any water contamination. A flow of ultrapure nitrogen was also maintained through the chamber at all times during the growth process. The flow rate of the nitrogen was adjusted to fine tune the evaporation rate of the ethanol colloidal suspension. All crystals were grown at room temperature (22–23 °C). Typical sample growth rates were approximately 150 μm/h.

The size and size distribution of the colloids used to make photonic crystal films were measured using scanning electron microscopy (SEM). The images were acquired from the same location on the sample from which optical spectra were previously acquired. Typically, five SEM images were col-

lected within a circle of diameter 200 microns. Each image used for sizing contained approximately 60 colloids. Since the colloids touch their nearest neighbors in a crystalline lattice, particle sizing by automated digital analysis software (ImagePro, Digital Micrograph) returned diameters smaller than the true value by up to 15%. In order to minimize such systematic errors these measurements were performed manually, reducing the errors to less than 1%. The average sphere diameters of all the suspensions fell in the range of 250–350 nm. The sphere size distributions, δ, of the suspensions varied from 3% (monodisperse) to 10% (polydisperse). Here, we define the parameter δ as the ratio of the standard deviation of the sphere diameters to the mean diameter.

The colloidal crystals thus prepared were characterized in two ways. The first method involved measuring the reflection and transmission spectra at specific points on the sample, using a microscope-enhanced uv-visible spectrometer [73]. An Olympus BX60 microscope was coupled to an ISA Jobin Yvon-Spex HR460 monochromator. The monochromator had a liquid nitrogen cooled CCD detector and could scan wavelengths from 400 nm to 1050 nm. The system was capable of measuring spectra in both reflection and transmission modes. Three objectives ($20\times, 50\times, 100\times$) and an internal field stop allowed the spot size to be varied from 50 μm to 1100 μm on the sample surface. Since the field stop is placed in the image plane, the collimation of the system in unchanged for any change in the field stop aperture. All measurements were performed at normal incidence along the [111] direction of the fcc lattice. In order to minimize the cone angle of collection to under 5° (to avoid detecting light scattered from planes other than [111]) an external aperture was used to reduce the effective numerical aperture to 0.1. The sample to be measured was placed on a stage with *x*-*y* translation. The stage had a measurement accuracy of 100 μm in both axis directions, though we have found that the repeatability of translation fell within 40 μm. The reference spectrum for the reflection and transmission measurements were obtained using an aluminum-sputtered glass slide and a plain glass slide, respectively. Several positions on each sample were selected for measurements. The coordinates of the positions were noted for subsequent SEM imaging. At each position the reflection spectrum was acquired for spot sizes of 50, 100, 150, 200, 220, 300, 440, 500, 1000, and 1100 μm and the transmission spectrum was obtained for spot sizes of 220, 440, and 1100 μm.

The second characterization procedure involved structural analysis from SEM imaging. Since the coordinates at which the optical spectra were taken were known, the same positions could be located on the sample under the SEM to within 10 μm. Thus, information extracted from structural analysis could be directly correlated to the optical spectra. At each position on the sample 10 top-down images were captured. From these images sphere size and lattice information were extracted.

In order to obtain a more quantitative description of disorder in the crystal structure, we performed a two-dimensional radial distribution analysis of the SEM images. This involved the calculation of the dimensionless pair correlation function (PCF), $g(r)$ [74],

$$g(r) = \frac{1}{\langle \rho \rangle} \frac{dn(r, r+dr)}{da(r, r+dr)}.$$

The PCF is a two-dimensional statistical mapping of the distances between the centers of pairs of colloids. It is evaluated by counting the number of spheres dn that lie within a spherical shell, dr, of radius r from an arbitrary origin. This is repeated for a range of radii and many arbitrary spheres selected as the origin. The statistical average of these numbers, normalized with respect to the average particle number density $\langle \rho \rangle$ and the sampling area $da = 2\pi r dr$ for a particular radial distance r, gives the pair correlation function, $g(r)$. The value of $g(r)$ is large when the distance, r, happens to coincide with a particular FCC lattice distance. Just before and beyond these distances the probability of encountering spheres is much smaller (since spheres cannot overlap). Hence we expect the PCF to consist of periodic peaks and dips. At distances larger than a characteristic correlation length, the short-range order breaks down. Since the correlation is lost, the number of particles within a given sampling volume is just the average particle density. Thus $g(r)$ converges to unity for large values of r. A highly ordered lattice results in a PCF with many oscillation. We obtain a quantitative measure of the correlation length by extracting the full width at half maximum (FWHM), κ, of the first peak of the Fourier transform of $g(r)-1$. A small value of κ indicates persistent oscillations in $g(r)$, and therefore a well-ordered lattice.

The structural disorder from SEM images of colloidal crystals could be quantified by obtaining the PCF using the procedure described previously [75,76]. The first step to calculating the PCF was to find the center coordinates of all the spheres in a given image, using image analysis software such as Digital Micrograph (Gatan Inc.). Because the results are sensitive to the details of the data processing, we describe here our approach to developing a protocol that most accurately determines the sphere coordinates. First the image was processed using a rank minimum filter. This took the pixels in a defined neighborhood and filtered out all but the brightest pixel resulting in a flattened image in which the spheres were separated. The spheres were then isolated using an automated thresholding process built into the software. Images used for PCF determination typically contained 2500 separated spheres. Several images were analyzed for each position on a particular sample. Figure 2 shows one such image with the coordinates of the spheres extracted. The dark filled circles indicate the position of the spheres as extracted from the software. It is evident, from the overlap of the extracted coordinates and the actual image, that the mapping of coordinates to spheres is very good.

Once the center coordinates of the spheres were found, the PCF was calculated, as described above. The outer circle in Fig. 2(a) shows the maximum radius for which the PCF was calculated for this image. This was determined as the shortest distance from the center to the edge of the image. The subset of colloids near the center of the image that are circled were used as the origin points. The results from all of these origin points were averaged to obtain the final PCF. Figure 2(b) shows the calculated PCF from the image in Fig.

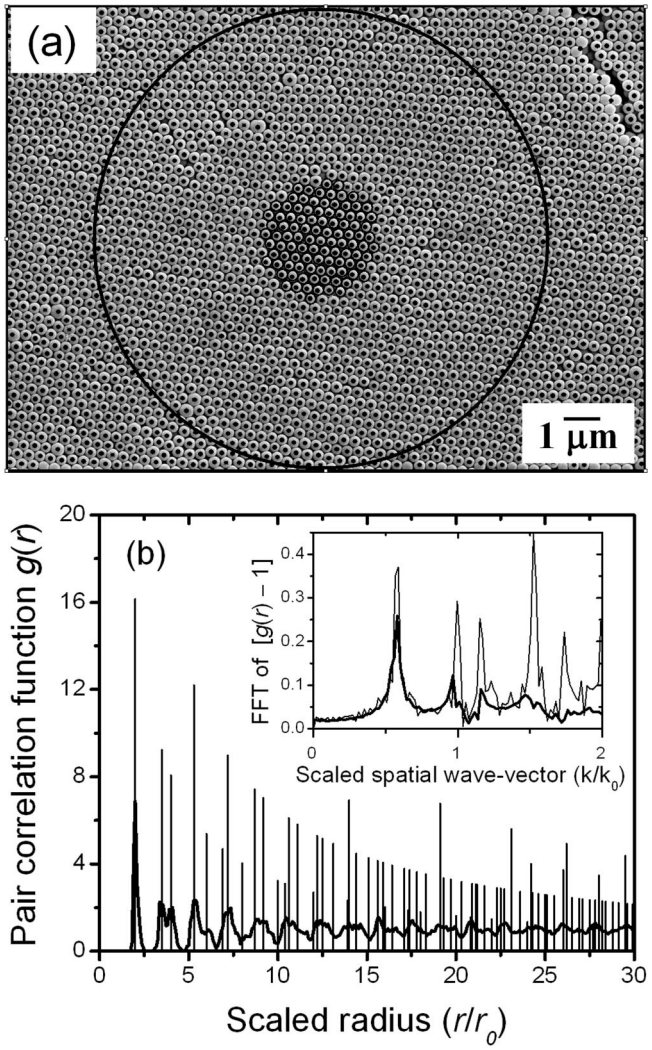

FIG. 2. An illustration of the method used to determine the pair correlation function. (a) Top-down SEM image of a [111] crystal surface with the center coordinates of the colloids extracted (dark filled circles) and mapped back onto the image. The outer black ring shows the maximum area of the image used for the calculation. This crystal was fabricated with spheres having a size distribution $\delta = 5.5\%$. The small number of spheres used to compute the pair correlation function are indicated by the collection of circles at the center of the image. (b) The pair correlation function computed from the above image (solid line) plotted against the scaled radius r/r_0, where r_0 is the mean sphere radius. Also shown is the series of delta functions which represent the PCF for an infinite perfect hexagonal lattice. The inset shows the Fourier transforms of these two PCFs. The thin line, the PCF for the ideal lattice, is computed for a lattice of finite size in order to make accurate comparisons with the PCFs extracted from finite SEM images. We use κ, the width of the first peak of this Fourier transform, as a measure of the degree of structural order shown in the SEM image.

2(a) (thick solid line) and also from a perfectly ordered triangular crystal lattice. In the case of the perfect lattice, the probability of finding a sphere at a particular location is known exactly, for arbitrary distance from the origin. Hence, $g(r)$ is a series of delta functions. The PCF for the actual colloidal crystal shows a series of broader peaks. However,

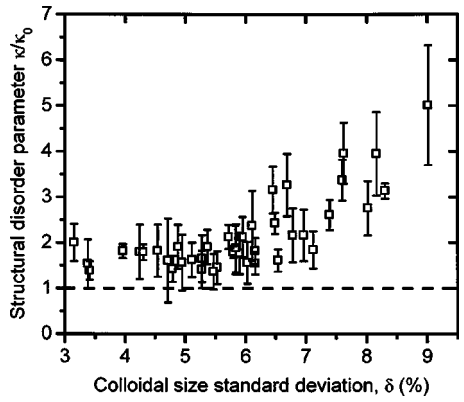

FIG. 3. Variation of two-dimensional order with colloidal size distribution. κ/κ_0 is the structural order parameter defined as the full width at half maximum of the first peak of the Fourier transform of the pair correlation function, normalized as described in the text. δ is the colloidal size distribution.

the similarity between the idealized calculation and the measured PCF is clear, particularly for smaller values of r. The persistent oscillations in the experimental curve indicate that the structural correlation was preserved over a long range. The inset [Fig. 2(b)] shows the Fourier transforms of the PCFs for the ideal and real crystals.

III. RESULTS AND DISCUSSION

We controlled the structural disorder in colloidal crystals by varying the size distribution of the colloidal solutions used to form the crystals. We characterize structural order quite broadly here; it is defined as the full width at half maximum (FWHM) of the first peak of the Fourier transform of the PCF. Thus this general structural order is best described as an "in-plane" parameter as it is derived from images of only the top layer of the films. We compute the values of κ normalized with respect to the result that would be obtained from a perfect crystal of the same dimensions, imaged with the same field of view. Therefore a value of $\kappa/\kappa_0 = 1$ would indicate a colloidal crystal that is essentially perfect in its two-dimensional structural order on the length scale of the size of the imaged region. Figure 3 shows this structural order parameter as a function of the colloidal size distribution δ.

These data show that colloidal size distribution has a powerful influence on the structural order of a colloidal crystal formed from controlled drying. Between $\delta = 3\%$ and 6% the colloidal crystals are near perfect, with a κ/κ_0 of about 1.5. Above $\delta = 6\%$, the in-plane structural disorder increases roughly linearly until at 9% the structural disorder is 5 times worse than a perfect crystal. The fact that κ saturates at $\sim 1.5\kappa_0$ for $\delta < 6\%$, and not at $\kappa = \kappa_0$, indicates that this value reflects the actual degree of order of the samples, and is not merely an artifact resulting from the finite area sampled by the SEM images. We conclude that a size distribution less than 6% ensures that the crystals have a reasonable degree of two-dimensional lattice order. Moreover, decreasing the size distribution beyond 6% does not lead to dramatic improve-

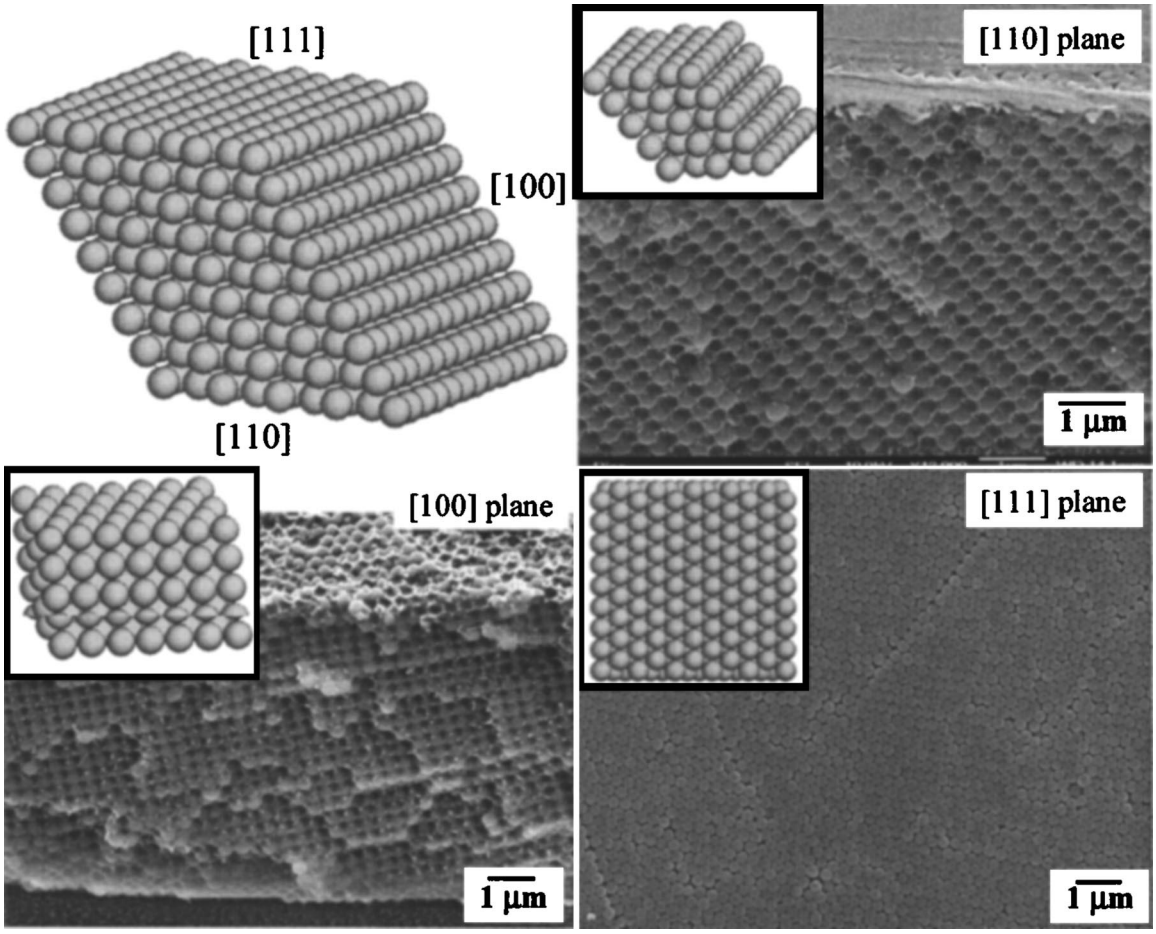

FIG. 4. Cross-sectional SEM images of a colloidal crystal having a size distribution of 4%. The crystal shows [110], [100], and [111] facets revealing it to be face-centered cubic (fcc). The insets corresponding to the images are cleaved images of a model fcc crystal. These cross-sectional views show no evidence of stacking faults.

ments in the in-plane structural order. As we show below, decreasing δ below 6% does lead to a slight decrease in the mean defect density, an effect too small to be evident in Fig. 3.

In addition to the in-plane structural disorder, we also evaluated whether these materials were disordered in planes perpendicular to the (111) plane. Stacking faults are a common form of disorder in crystalline solids and their presence in gravity sedimented colloidal crystals has been studied by others [17,48,52,56]. Figure 4 shows cross-sectional views of a typical colloidal crystal produced through controlled drying methods. The size distribution for this particular sample is 4%. The lattice was infiltrated with a polymer (polystyrene) to provide mechanical support for cross-sectional analysis. Though there are some spheres missing due to the cleaving process in sample preparation, the cross sections along the $\langle 100 \rangle$ and $\langle 110 \rangle$ lattice planes are visible. These images, typical of many crystals that we have studied, clearly demonstrate that crystals formed using the controlled drying method exhibit a negligible density of stacking faults, and confirm that the lattice structure is face-centered cubic (fcc). This is to be distinguished from colloidal crystals formed via other methods, which may produce a higher density of stacking faults [58]. Moreover, the crystal density in our films is uniform throughout the entire depth of the crystal and missing spheres are no more prevalent closer to the substrate than on the surface. These results are consistent with earlier discussions of crystals grown using a modification of this technique [26]. For these reasons, we expect that the influence of stacking faults on the optical spectra is small, compared to that of other types of defects. So, the remainder of this article focuses on disorder arising from in-plane defects.

Several specific types of crystal defects contribute to the in-plane structural disorder as parametrized by κ/κ_0. Line and point defects are the most visually apparent features in colloidal crystal images. Fractional displacement of an entire section of the crystal is a signature of a line defect, whereas point defects are single sphere vacancies in an otherwise perfect crystal. Using the top-down SEM views, we have determined the average density of both point and line defects. These results are shown in Fig. 5, as a function of sphere size distribution δ, along with representative views of the two types of defect. For the most uniform colloidal crystals ($\delta < 4\%$) we found defect densities an order of magnitude less ($\sim 10^6$ cm^{-2}) than those reported in earlier studies of planar colloids [53]. It is apparent from the data that line defects are more abundant than point defects, typically by a factor of 2. We also found that the density of these defects weakly in-

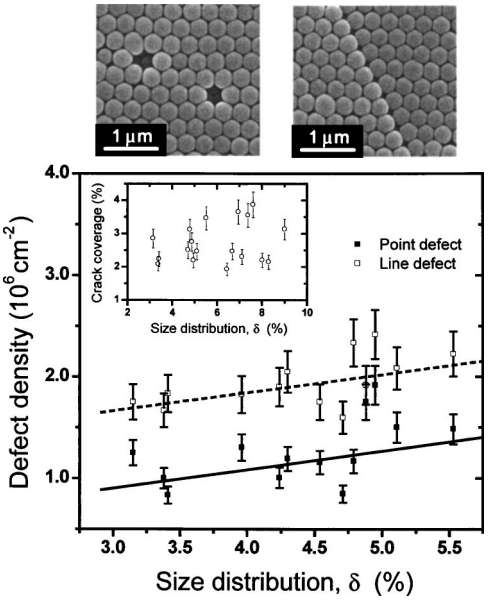

FIG. 5. Estimation of in-plane defect densities as a function of colloidal size distribution. The SEM images show examples of line and point defects. The defect densities for the line (open square) and point (solid square) defects are fitted to a linear regression. These densities are about an order of magnitude less than those previously reported for colloidal crystals [53]. The inset analyzes crack densities from drying processes and plots the percentage of the surface area of the crystal occupied by cracks. As expected, there is no discernable trend with size distribution. The average crack coverage is approximately $2.7 \pm 0.6\%$ per unit area.

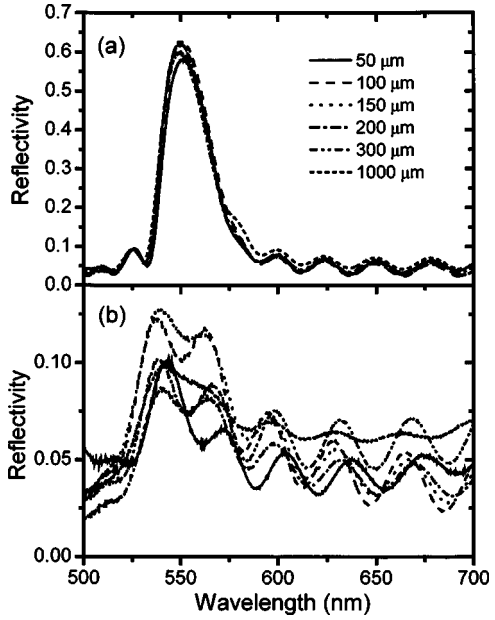

FIG. 6. Normal incidence reflectivity spectra as a function of spot size. (a) Spectra from a crystal with $\delta = 5.7\%$. The different spectra overlap with minimal fluctuation in the peak reflectivity (a variation in the peak amplitude of less than 3%). (b) Spectrum from a crystal with $\delta = 9.0\%$. These spectra show large variations in shape, with significant fluctuations in the peak reflectivity (variation greater than 13%), as well as substantial variations in crystal thickness. The legend applies to both (a) and (b).

creases as the size distribution parameter increases. This weak trend is too small to have a significant impact on the results of the PCF analysis (see Fig. 3), and is therefore also not likely to have a strong impact on the optical properties of the films near the first stop band. This is confirmed by our optical studies, discussed further below.

Another source of disorder affecting the optical properties of colloidal crystals are cracks that develop during drying of the films. After the colloids are deposited on the glass substrate during the growth phase, drying cracks develop as the solvent evaporates. We expect that the size and number of these cracks should be independent of the colloid size distribution, since they are formed after the deposition process. The cracks, unlike grain boundaries, do not destroy the overall order of the crystal; they only introduce small gaps in an otherwise uniform single crystal. In order to estimate the significance of cracks, we digitally processed the SEM images to extract the surface area coverage of the cracks in a given image. It should be noted that the very process of imaging these crystals in an ultrahigh vacuum causes the cracks to expand. Hence the data presented here represent upper limits of crack coverage (i.e., the worst case). The inset in Fig. 5 shows the percentage of crack coverage per unit area as a function of colloidal size distribution. The plot shows no discernable trend with size distribution, as expected. On average only about 2.7% of the image area were cracks. These were generally spaced by 10 to 50 microns.

Disorder in colloidal crystals leads to many distinctive changes in the optical properties. This is apparent in Fig. 6, which displays the reflection spectra as a function of illumination spot size for two crystals with very different degrees of order. The figure shows superimposed reflection spectra for two crystals, formed with spheres having $\delta = 5.7\%$ (upper) and $\delta = 9.0\%$ (lower), respectively. The spectra were measured at the same central position on each sample, and spot sizes were varied from 50 μm to 1 mm. The more monodisperse sample (5.7%) shows spectra that are identical and independent of spot size. The more polydisperse film, on the other hand, exhibits more evidence of structural disorder. As can be seen from the variability of the spectra, the optical spot size has a drastic effect on the appearance of the spectrum in this case. In contrast to the case of the $\delta = 5.7\%$ sample, the peak reflectivity changes significantly over the range probed in the experiment ($\sim 13\%$). Also, the peak reflectivity for smaller spot sizes (100 and 150 μm) is larger than when measured with larger spot sizes, suggesting that the domain size is less than 150 μm. It is clear that a photonic crystal formed with polydisperse colloids has poor optical uniformity even in regions as small as 150 μm.

Having obtained optical spectra from specific regions of the crystal that have also been characterized for structural disorder, it is now possible to correlate the optical properties and the structural uniformity of the colloidal crystals as a function of the size distribution of the colloids. Figure 7 shows reflection spectra, SEM images, and PCFs for four typical samples with different size distributions. The horizontal axes of the reflection spectra have been shifted so as to facilitate comparison of samples with varying radii. On this normalized frequency axis, the lowest stop band lies at

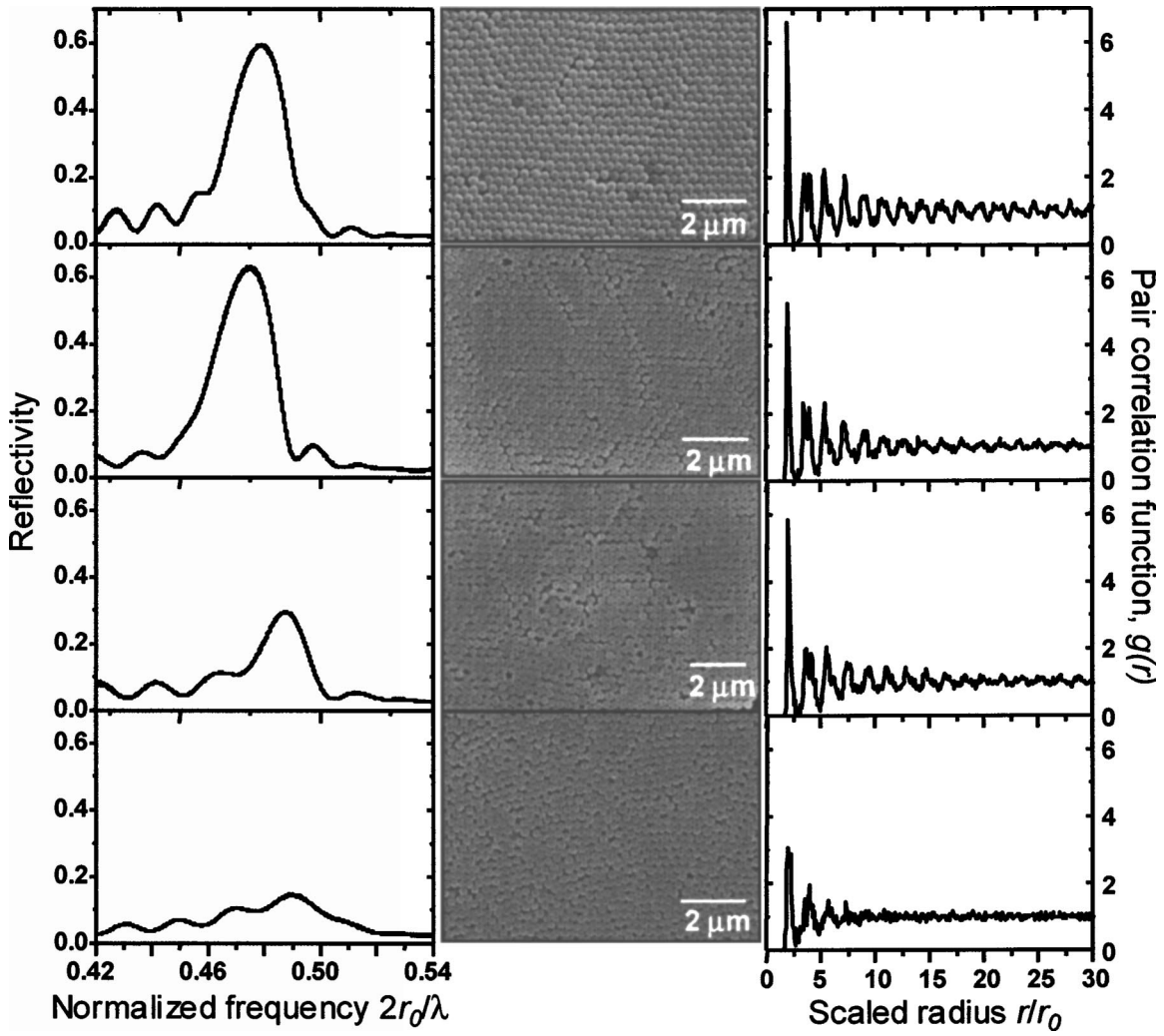

FIG. 7. Qualitative correlation of the optical spectrum and structural disorder with increased polydispersity of the colloids. Each row represents data from one particular spot on a crystal. The first column shows the reflectivity spectrum. The horizontal axis is normalized with respect to the sphere diameter, $2r_0$. In these frequency units, the stop band occurs at 0.48. The second column is the corresponding top-down SEM image. The images are magnified for clear viewing. The last column represents the pair correlation function of the corresponding SEM image plotted against a normalized radial distance. From top to bottom, the size distributions are $\delta = 4.9\%$, 5.7%, 6.5%, and 7.4%.

$2r_0/\lambda = 0.48$. There is a dramatic change in the reflection spectrum as the size distribution parameter δ increases. However, size distribution has a smaller effect on the appearance of the materials in the SEM images; the top and bottom images, for example, do not seem so drastically different on casual inspection, as compared to the reflection spectra. However, when the PCF is extracted from these images, the subtle but important differences in structural order are more obvious. In particular, the number of oscillations in the PCF decreases as δ increases, clearly indicating a deterioration of the in-plane structural order.

A more detailed analysis of the optical properties shows that the two features of the optical reflectivity that are most sensitive to disorder are the peak reflectivity and the full width at half maximum (FWHM) of the stop band. Figure 8(a) shows the peak reflectivity of the stop band as a function of the sphere size distribution, for constant optical spot size. It is known that the peak of the reflection spectrum increases exponentially with increasing film thickness [53], as long as the film is thicker than a critical thickness of $N_c \approx 13$ layers of colloids [62]. Because of this strong thickness dependence, comparisons between samples of different thickness are difficult unless the results are first normalized in some way. Since all of our samples are thicker than the critical thickness, we can correct our measured peak reflectivities to facilitate such comparisons. In Fig. 8(a), we have normalized all of our measured data using this exponential scaling, to show what each of their reflectivities would be if the films all had a thickness of 30 layers. For reference, an ideal crystal with 30 layers should reflect about 80% of the incident light at the center of the stop band. We observe that the best samples (those with the smallest values of δ) indeed approach this ideal value. Further, it is evident that there is a critical size distribution, $\delta = 6\%$, beyond which the reflectivity at the center of the stop band drops rapidly. For the most polydisperse crystals the peak reflectivity falls to less than 10%. For smaller size distributions the peak reflectivity is independent of δ, within our experimental uncertainty.

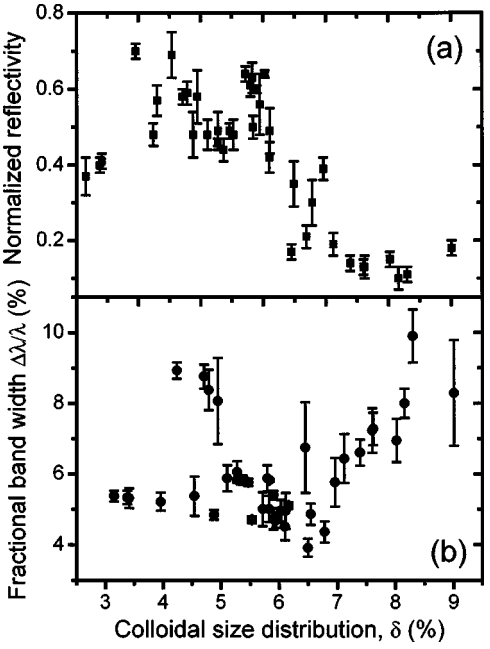

FIG. 8. Quantitative trends in stop band parameters as a function of colloidal size distribution. (a) Peak reflectivity, normalized to 30 layers as described in the text. A perfect lattice has a peak reflectivity of 0.8 for a thickness of 30 layers. (b) FWHM of the reflection peak, normalized to 30 layers. A perfect lattice has a fractional bandwidth of 5.8%, as predicted by both scalar wave and transfer matrix theories.

Figure 8(b) shows the fractional bandwidth ($\Delta\lambda/\lambda$) as a function of the sphere size distribution. Because the fractional bandgap is only dependent on the crystal structure (it is invariant for a given dielectric contrast, for fcc colloidal crystals), it is an ideal parameter for comparing the uniformity of different samples. Here, a normalization procedure is again required for meaningful comparisons of samples with different film thickness. In this case, the dependence of the FWHM on the film thickness is not so simple as an exponential relationship. Instead, we have used the theoretically predicted relation derived from the scalar wave approximation (SWA), which has been shown to provide a reasonably good description of the variation of bandwidth with thickness [62,77]. Despite the approximate nature of the SWA, we expect that this normalization procedure should be valid, particularly since the variation of FWHM with thickness is not very strong for samples thicker than N_c [62]. As above, we normalize the measured FWHM to the value predicted for a crystal with a thickness of 30 layers, and then divide by the central wavelength in order to obtain the normalized $\Delta\lambda/\lambda$. The SWA predicts that the spectrum of a perfect 30 layers crystal should have a fractional bandwidth of 5.8%. This value is the same as the result obtained from a numerical simulation based on the transfer matrix method [78]. As shown in Fig. 8(b), the fractional bandwidth is constant at approximately 5.5% for $\delta < 6\%$, slightly lower than the value of 5.8% for a perfect crystal. For $\delta > 6\%$ the fractional bandwidth increases approximately linearly with further increase in disorder. One way to understand this result is to consider that in a photonic crystal, increasing the level of disorder can lead to significant changes in the photon density of states. The local density of states, which shows a pseudogap mainly along the [111] direction, is a key property in these systems. As a perfect crystal experiences a small increase in disorder, propagating modes may be introduced near the edges of the partial band gap. This may cause the pseudogap to close slightly resulting in the observed reduction of the bandwidth for low levels of disorder, i.e., $\delta < 6\%$. However, at a certain point the number of states inside the partial gap may be sufficient to fill the gap. Since the total number of states is constant, one may expect that the density of states near (but not in) the gap could decrease while the number inside the gap increases. As a result, the dip in the density of states may become shallower and broader. This could explain why the observed bandwidth increases as the degree of disorder increases beyond $\delta = 6\%$. A similar effect has been described in recent theoretical studies of templated photonic crystals [49].

There are also a few anomalous but experimentally consistent data points with $\Delta\lambda/\lambda$ values in the range of 8–9 %. In assessing the origin of these data points, we have considered whether stacking faults could be increasing the bandwidth of the partial gap in monodisperse samples. It has been shown in theoretical investigations that stacking faults in an otherwise perfectly ordered crystal can broaden the full band gap [48]; however, our samples have a low incidence of stacking faults (see Fig. 4). We also note that this theoretical work assumed stacking faults on the order of 20%, which is clearly significantly larger than what we observe, or indeed what is seen in crystals grown using any controlled drying method [26]. In addition, even for this large fault density the effect on the partial gap was much smaller than the observed effect. It seems unlikely that stacking faults could produce the broadening observed in the bandwidth of these crystals. At present we do not have an explanation as to why the observed bandwidth in some monodisperse samples is nearly twice the predicted value for the very uniform crystals.

Although we are not able to confirm that subtle changes in the midgap density of states are responsible for the variation of the fractional bandwidth in near-perfect crystals, this data does suggest that sphere size distribution is an important parameter to control when generating colloidal crystal templates for photonic applications. For our particular growth conditions, there is a critical transition at $\delta = 6\%$ for the fabrication of high-quality colloidal crystals. This result is reflected in several independent measurements of both the structural and optical quality of the materials [see, for example, Fig. 3 and 8(a)]. It demonstrates for the first time that to achieve optimal optical properties, the size distribution of the starting colloidal materials must be below a certain critical value. Theoretical studies have indicated that the full gap (between the 8th and 9th bands) is more sensitive to disorder than is the lower gap investigated here [48,49], so it is likely that even smaller values of δ are required for studies which rely on this higher gap. We note that starting with monodisperse colloids is a necessary condition for growth of high-quality films, but of course it is also necessary to carefully control the growth conditions, as described earlier. While much of the recent work on colloidal crystals has focused specifically on the optical properties near the stop band, an equally important parameter to characterize is the diffuse

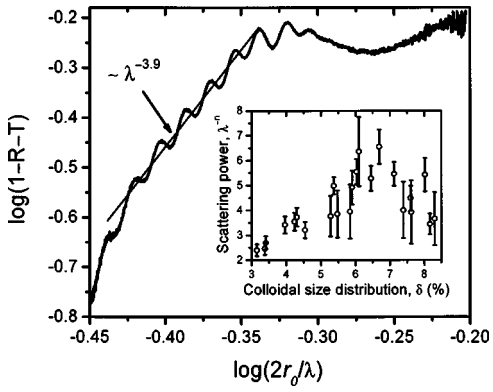

FIG. 9. A plot of the diffuse scattering spectrum of a film formed with colloids having δ=8.2%. The scattering spectrum, plotted on a $\log_{10}$ scale, is defined as $S(\lambda)=1-R-T$, where R and T are the reflectivity and the transmissivity measured at the same location on the crystal. The horizontal axis is the normalized frequency $2r_0/\lambda$, as in Fig. 7, also plotted on a $\log_{10}$ scale. The long wavelength region of the spectrum approximately follows Rayleigh's law, superimposed on the usual Fabry-Pérot oscillations. A linear fit to this region illustrates the power law behavior. In contrast, the short wavelength region is not well described by a power law. The inset shows the power law exponent, extracted from the long-wavelength regions, as a function of colloidal size distribution.

broadband scattering [79]. In particular, the majority of published spectra have exhibited a diffuse background, increasing with decreasing wavelength as roughly a power law. Often this spectral feature is simply fitted to a power law, and subtracted from the experimental data prior to further processing. This broadband feature has generally been interpreted as scattering from random defects within the otherwise ordered crystal [80], but there has been no systematic study of its variation with crystalline order.

We have evaluated the scattering spectrum as a function of the degree of disorder, in order to better understand its origins. The spectrum of the scattered radiation is obtained from $S(\lambda)=1-R(\lambda)-T(\lambda)$, where $R(\lambda)$ and $T(\lambda)$ are the reflection and transmission coefficients, respectively, measured at the same location on the sample. Figure 9 shows a representative scattering spectrum of a colloidal crystal sample with δ=8.2%, plotted on a log scale. The horizontal axis is the normalized frequency $2r_0/\lambda$, as in Fig. 7, also plotted on a log scale.

We expect that the nature of the scattering profile can provide information about the size of the defects responsible for diffuse scattering. From Fig. 9 it is apparent that for wavelengths longer than the Bragg wavelength, the scattering approximately follows Rayleigh's law. The Rayleigh scattering regime is generally assumed to apply only to very small scatterers, when $kd<0.1$, where d is the diameter of the scatterer [81]. This implies that in colloidal crystals, the scattering site is less than 20 nm in size. The imperfections in this size range include the variations in the sphere diameters (and the sizes of the interstitial regions), surface roughness and the random variations in the sphere positions. On the short wavelength side of the stop band, the scattering is evidently not well described by a simple power law. It is possible that the contributions to diffuse scattering in this regime include effects from larger scatterers in the sample, e.g., drying cracks or line defects.

We have attempted to describe the long-wavelength scattering for all of our samples using a power law of the form λ^{-n}, where n is the scattering power ($n=4$ for Rayleigh scattering). The inset to Fig. 9 shows the extracted value of this exponent as a function of size distribution. Although there is considerable variation in the results, the general trend is that $n<4$ for smaller size distributions, and $n>4$ for larger size distributions. This is consistent with a simple Mie theory simulation, which predicts that point vacancies result in a scattering power of $n<4$. These results suggest that, for crystals with a greater degree of disorder ($\delta>5-6$ %) the primary source of scattering is not from sphere vacancies or stacking faults, but from disorder resulting from the finite sphere size distributions. This would incorporate both size and site randomness. However for small δ values (<5%), the disorder due to site and size randomness of the spheres is minimized due to the monodispersity of the colloids. Here, the primary source of scattering is point defects, i.e., structures similar in size to the spheres such as vacancies.

IV. CONCLUSIONS

In conclusion, we have carried out an in-depth study on the role of sphere size disorder on the optical properties of colloidal crystals. We have estimated the density of both line and point defects for samples grown using the controlled drying method, and obtained values substantially lower than those previously reported for other types of colloidal crystals. We have shown quantitatively how the the sphere size distribution influences both the optical and structural properties of colloidal films; in particular, to generate ordered crystals requires a critical value in size distribution ($\delta\sim6$%) beyond which the lowest frequency stop band deteriorates rapidly. Also for very monodisperse colloids the main source of scattering is from point defects, which suggests that in well ordered crystals stacking faults and sphere size randomness play secondary roles insofar as their effect on the optical spectrum. We also report an anomalous behavior in the variation of the width of the optical stop band with δ, which may result from defect-induced variations in the photon density of states near the band edges. These data improve our understanding of the connection between structural and optical properties in colloidal photonic crystals, and suggest methods to improve their fabrication.

ACKNOWLEDGMENTS

The authors would like to acknowledge Silvia Rubio for her contributions during the early phase of this work. The authors would also like to thank William Bosworth for his assistance with the measurements of the colloid size distributions. This work was supported in part by the National Science Foundation (ECS-0103174) and by the R. A. Welch Foundation (C-1538).

[1] E. Yablonovitch, Phys. Rev. Lett. **58**, 2059 (1987).
[2] S. John, Phys. Rev. Lett. **58**, 2486 (1987).
[3] J. D. Joannopoulos, R. D. Meade, and J. N. Winn, *Photonic Crystals: Molding the Flow of Light* (Princeton University Press, Princeton, NJ, 1995).
[4] T. F. Krauss, R. M. DeLaRue, and S. Brand, Nature (London) **383**, 699 (1996).
[5] O. Painter, R. K. Lee, A. Scherer, A. Yariv, J. D. O'Brien, P. D. Dapkus, and I. Kim, Science **284**, 1819 (1999).
[6] E. Chow, S. Y. Lin, S. G. Johnson, P. R. Villeneuve, J. D. Joannopoulos, J. R. Wendt, G. A. Vawter, W. Zubrzycki, H. Hou, and A. Alleman, Nature (London) **407**, 983 (2000).
[7] M. E. Zoorob, M. D. B. Charlton, G. J. Parker, J. J. Baumberg, and M. C. Netti, Nature (London) **404**, 740 (2000).
[8] C. Weisbuch, H. Benisty, M. Rattier, C. J. M. Smith, and T. F. Krauss, Synth. Met. **116**, 449 (2001).
[9] M. Imada, A. Chutinan, S. Noda, and M. Mochizuki, Phys. Rev. B **65**, 195306 (2002).
[10] Y. Akahane, T. Asano, B. S. Song, and S. Noda, Nature (London) **425**, 944 (2003).
[11] D. N. Christodoulides, F. Lederer, and Y. Silberberg, Nature (London) **424**, 817 (2003).
[12] A. Chutinan, S. John, and O. Toader, Phys. Rev. Lett. **90**, 123901 (2003).
[13] R. Colombelli, K. Srinivasan, M. Troccoli, O. Painter, C. F. Gmachl, D. M. Tennant, A. M. Sergent, D. L. Sivco, A. Y. Cho, and F. Capasso, Science **302**, 1374 (2003).
[14] P. Russell, Science **299**, 358 (2003).
[15] Y. G. Roh, S. Yoon, S. Kim, H. Jeon, S. H. Han, Q. H. Park, and I. Park, Appl. Phys. Lett. **83**, 231 (2003).
[16] S. Y. Lin, J. G. Fleming, D. L. Hetherington, B. K. Smith, R. Biswas, K. M. Ho, M. M. Sigalas, W. Zubrzycki, S. R. Kurtz, and J. Bur, Nature (London) **394**, 251 (1998).
[17] H. Miguez, F. Meseguer, C. Lopez, A. Mifsud, J. S. Moya, and L. Vazquez, Langmuir **13**, 6009 (1997).
[18] A. van Blaaderen, R. Ruel, and P. Wiltzius, Nature (London) **385**, 321 (1997).
[19] J. Wijnhoven and W. L. Vos, Science **281**, 802 (1998).
[20] Z. D. Cheng, W. B. Russell, and P. M. Chaikin, Nature (London) **401**, 893 (1999).
[21] S. A. Johnson, P. J. Ollivier, and T. E. Mallouk, Science **283**, 963 (1999).
[22] O. D. Velev, A. M. Lenhoff, and E. W. Kaler, Science **287**, 2240 (2000).
[23] P. Jiang, J. F. Bertone, K. S. Hwang, and V. L. Colvin, Chaos **11**, 2132 (1999).
[24] S. H. Park, B. Gates, and Y. N. Xia, Adv. Mater. (Weinheim, Ger.) **11**, 462 (1999).
[25] R. M. Amos, J. G. Rarity, P. R. Tapster, T. J. Shepherd, and S. C. Kitson, Phys. Rev. E **61**, 2929 (2000).
[26] Y. A. Vlasov, X. Z. Bo, J. C. Sturm, and D. J. Norris, Nature (London) **414**, 289 (2001).
[27] S. G. Romanov, A. V. Fokin, H. M. Yates, M. E. Pemble, N. P. Johnson, and R. M. De La Rue, IEE Proc.: Optoelectron. **147**, 138 (2000).
[28] M. E. Turner, T. J. Trentler, and V. L. Colvin, Adv. Mater. (Weinheim, Ger.) **13**, 180 (2001).
[29] P. Jiang, J. F. Bertone, and V. L. Colvin, Science **291**, 453 (2001).
[30] Q. B. Meng, C. H. Fu, Y. Einaga, Z. Z. Gu, A. Fujishima, and O. Sato, Chem. Mater. **14**, 83 (2002).
[31] F. Meseguer, A. Blanco, H. Miguez, F. Garcia-Santamaria, M. Ibisate, and C. Lopez, Colloids Surf., A **202**, 281 (2002).
[32] L. Y. Hao, M. You, X. Mo, W. Q. Jiang, Y. R. Zhu, Y. Zhou, Y. A. Hu, X. M. Liu, and Z. Y. Chen, Mater. Res. Bull. **38**, 723 (2003).
[33] B. Gates, Y. D. Yin, and Y. N. Xia, Chem. Mater. **11**, 2827 (1999).
[34] P. Jiang, K. S. Hwang, D. M. Mittleman, J. F. Bertone, and V. L. Colvin, J. Am. Chem. Soc. **121**, 11630 (1999).
[35] A. A. Zakhidov, R. H. Baughman, Z. Iqbal, C. X. Cui, I. Khayrullin, S. O. Dantas, I. Marti, and V. G. Ralchenko, Science **282**, 897 (1998).
[36] P. Jiang, J. Cizeron, J. F. Bertone, and V. L. Colvin, J. Am. Chem. Soc. **121**, 7957 (1999).
[37] O. D. Velev, P. M. Tessier, A. M. Lenhoff, and E. W. Kaler, Nature (London) **401**, 548 (1999).
[38] H. W. Yan, C. F. Blanford, B. T. Holland, M. Parent, W. H. Smyrl, and A. Stein, Adv. Mater. (Weinheim, Ger.) **11**, 1003 (1999).
[39] K. M. Kulinowski, P. Jiang, H. Vaswani, and V. L. Colvin, Adv. Mater. (Weinheim, Ger.) **12**, 833 (2000).
[40] J. Aizenberg, P. V. Braun, and P. Wiltzius, Phys. Rev. Lett. **84**, 2997 (2000).
[41] K. M. Chen, X. P. Jiang, L. C. Kimerling, and P. T. Hammond, Langmuir **16**, 7825 (2000).
[42] Y. H. Ye, S. Badilescu, V. V. Truong, P. Rochon, and A. Natansohn, Appl. Phys. Lett. **79**, 872 (2001).
[43] E. Kumacheva, R. K. Golding, M. Allard, and E. H. Sargent, Adv. Mater. (Weinheim, Ger.) **14**, 221 (2002).
[44] H. Miguez, S. M. Yang, and G. A. Ozin, Appl. Phys. Lett. **81**, 2493 (2002).
[45] Y. Yin, Z. Y. Li, and Y. Xia, Langmuir **19**, 622 (2003).
[46] S. Wong, V. Kitaev, and G. A. Ozin, J. Am. Chem. Soc. **125**, 15589 (2003).
[47] A. S. Dimitrov and K. Nagayama, Langmuir **12**, 1303 (1996).
[48] V. Yannopapas, N. Stefanou, and A. Modinos, Phys. Rev. Lett. **86**, 4811 (2001).
[49] Z. Y. Li and Z. Q. Zhang, Phys. Rev. B **62**, 1516 (2000).
[50] P. N. Pusey, W. Vanmegen, P. Bartlett, B. J. Ackerson, J. G. Rarity, and S. M. Underwood, Phys. Rev. Lett. **63**, 2753 (1989).
[51] M. M. Sigalas, C. M. Soukoulis, C. T. Chan, R. Biswas, and K. M. Ho, Phys. Rev. B **59**, 12767 (1999).
[52] E. A. Monroe, D. B. Sass, and S. H. Cole, Acta Crystallogr., Sect. A: Cryst. Phys., Diffr., Theor. Gen. Crystallogr. **25**, 578 (1969).
[53] Y. A. Vlasov, V. N. Astratov, A. V. Baryshev, A. A. Kaplyanskii, O. Z. Karimov, and M. F. Limonov, Phys. Rev. E **61**, 5784 (2000).
[54] J. Huang, N. Eradat, M. E. Raikh, Z. V. Vardeny, A. A. Zakhidov, and R. H. Baughman, Phys. Rev. Lett. **86**, 4815 (2001).
[55] V. N. Astratov, A. M. Adawi, S. Fricker, M. S. Skolnick, D. M. Whittaker, and P. N. Pusey, Phys. Rev. B **66**, 165215 (2002).
[56] J. P. Hoogenboom, D. Derks, P. Vergeer, and A. van Blaaderen, J. Chem. Phys. **117**, 11320 (2002).
[57] J. F. Lopez and W. L. Vos, Phys. Rev. E **66**, 036616 (2002).
[58] S. A. Asher, J. M. Weissman, A. Tikhonov, R. D. Coalson, and R. Kesavamoorthy, Phys. Rev. E **69**, 066619 (2004).
[59] P. A. Rundquist, P. Photinos, S. Jagannathan, and S. A. Asher,

J. Chem. Phys. **91**, 4932 (1989).
[60] P. A. Rundquist, R. Kesavamoorthy, S. Jagannathan, and S. A. Asher, J. Chem. Phys. **95**, 1249 (1991).
[61] S. Johnson and J. Joannopoulous, http://ab-initio.mit.edu/mpb, 1999.
[62] J. F. Bertone, P. Jiang, K. S. Hwang, D. M. Mittleman, and V. L. Colvin, Phys. Rev. Lett. **83**, 300 (1999).
[63] H. S. Sozuer, J. W. Haus, and R. Inguva, Phys. Rev. B **45**, 13962 (1992).
[64] K. Busch and S. John, Phys. Rev. E **58**, 3896 (1998).
[65] A. Blanco, E. Chomski, S. Grabtchak, M. Ibisate, S. John, S. W. Leonard, C. Lopez, F. Meseguer, H. Miguez, J. P. Mondia, G. A. Ozin, O. Toader, and H. M. van Driel, Nature (London) **405**, 437 (2000).
[66] S. H. Park and Y. N. Xia, Chem. Mater. **10**, 1745 (1998).
[67] O. D. Velev, T. A. Jede, R. F. Lobo, and A. M. Lenhoff, Chem. Mater. **10**, 3597 (1998).
[68] P. D. Yang, T. Deng, D. Y. Zhao, P. Y. Feng, D. Pine, B. F. Chmelka, G. M. Whitesides, and G. D. Stucky, Science **282**, 2244 (1998).
[69] B. T. Holland, C. F. Blanford, T. Do, and A. Stein, Chem. Mater. **11**, 795 (1999).
[70] G. Subramanian, V. N. Manoharan, J. D. Thorne, and D. J. Pine, Adv. Mater. (Weinheim, Ger.) **11**, 1261 (1999).
[71] O. D. Velev and A. M. Lenhoff, Curr. Opin. Colloid Interface Sci. **5**, 56 (2000).
[72] W. Stober, A. Fink, and E. Bohn, J. Colloid Interface Sci. **26**, 62 (1968).
[73] Y. A. Vlasov, M. Deutsch, and D. J. Norris, Appl. Phys. Lett. **76**, 1627 (2000).
[74] S. M. Allen and E. L. Thomas, *The Structure of Materials* (Wiley, New York, 1999).
[75] J. Ballato, J. DiMaio, E. Gulliver, D. G. Han, R. E. Riman, and D. L. Carroll, Opt. Mater. (Amsterdam, Neth.) **20**, 51 (2002).
[76] J. Ballato, J. DiMaio, T. D. Taylor, E. Gulliver, D. G. Han, R. E. Riman, and D. L. Carroll, J. Am. Ceram. Soc. **85**, 1366 (2002).
[77] D. M. Mittleman, J. F. Bertone, P. Jiang, K. S. Hwang, and V. L. Colvin, J. Chem. Phys. **111**, 345 (1999).
[78] D. Cassagne, A. Reynolds, and C. Jouanin, Opt. Quantum Electron. **32**, 923 (2000).
[79] A. Femius Koenderink and W. L. Vos, Phys. Rev. Lett. **91**, 213902 (2003).
[80] A. Femius Koenderink, M. Megens, G. van Soest, W. L. Vos, and A. Lagendijk, Phys. Lett. A **268**, 104 (2000).
[81] A. Ishimaru, *Wave Propagation and Scattering in Random Media* (Academic, New York, 1978).